



M Ű E G Y E T E M 1 7 8 2

Budapesti Műszaki és Gazdaságtudományi Egyetem

Budapest University of Technology and Economics

PÁL VÁSÁRHELYI DOCTORAL SCHOOL OF CIVIL ENGINEERING AND EARTH SCIENCES

DEPARTMENT OF STRUCTURAL MECHANICS

*DISCRETE ELEMENT ANALYSIS
OF HISTORIC MASONRY VAULTS AND DOMES*

SUMMARY

Chen Shipeng

SUPERVISOR

Prof. Katalin Bagi

2024 July

Introduction

Historic masonry vaults and domes are among the most remarkable parts of the architectural heritage in Europe and around the world. Many of these structures have survived for centuries or even millennia, despite the presence of minor or significant cracks. Therefore, appropriate strengthening solutions should be implemented to protect these structures. However, it is essential first to understand their mechanical behaviour, including cracking patterns, load-bearing capacity, and stability under loads (forces or support displacements), in order to select suitable strengthening or maintenance methods.

Masonry shells are composed of individual stone blocks or bricks, and their discrete construction strongly influences their mechanical response to static or kinematic loads. The failure of such structures is usually related to localized effects, such as a few cracked joints forming a hinge, or the crushing or sliding of a single voussoir. Traditional continuum-based methods, such as the Finite Element Method (FEM), are inefficient or even unable to describe these phenomena. The Discrete Element Method (DEM) can overcome this difficulty: after their material parameters are suitably calibrated, DEM codes can reliably simulate the mechanical behaviour.

This dissertation employs the Discrete Element Method (DEM) to analyze various masonry vaults and domes under quasi-static loads and support displacements. The numerical simulations were conducted using 3DEC, a software developed by Itasca Consulting Group, which has been widely used and thoroughly tested over decades for analyzing masonry structures. Utilizing 3DEC, I validated the theoretical predictions of crosswise tension resistance for general running bond patterns as well as 1:2 and 1:3 herringbone patterns. Furthermore, I examined the load-bearing capacity, cracking patterns or failure mechanisms, and the orientation of reactions at supports for different historic masonry vaults and domes. Additionally, I demonstrated the impact of the sign of Gaussian curvature on open vaults with square bays.

Thesis 1: Crosswise tension resistance in masonry shells with different bond patterns

1.1 Introduction

Classical approaches, e.g., Heyman’s limit state analysis, for analysing masonry shells often assume that masonry has no tensile resistance. This assumption is generally a safe approximation of historic structures where the mortar layers (if any) have fully lost cohesion. However, an increasing number of studies have demonstrated that masonry structures can exhibit significant tensile resistance if proper bond patterns are selected, even when the individual contacts do not resist tension. This tensile resistance (Figure 1.1) may arise, for example, from friction at the contacts or interfaces between blocks. Simon & Bagi (2016) quantitatively noted in DEM-simulated experiments that the friction between blocks considerably improves the strength of domes and decreases the necessary minimal thickness of the dome to carry its self-weight. Beatini et al. (2018) independently showed (also with DEM simulations) that the vertical pressure applied to each of the horizontal layers can provide hoop tension resistance in domes.

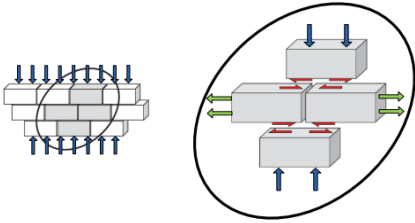


Figure 1.1. Explanation of the crosswise tensile resistance (Simon & Bagi, 2016).

1.2 Quantification of crosswise tension resistance for different bond patterns

In masonry vaults and domes, running bond and herringbone patterns (Figure 1.2) are the most-widely used bond patterns. By choosing suitable elementary cells and taking into account the force equilibrium and moment balance equilibrium equations, theoretical predictions were derived for general running bond, and 1:2 and 1:3 herringbone patterns. The crosswise tension resistance of straight-shifted and skew-shifted running bond patterns for $\alpha = 1/2, /3$ and $1/4$, is $\sigma_t = \mu \frac{\alpha b}{h} \sigma_c$. α denotes the ratio of shifting. The crosswise tension resistances of 1:2 herringbone and 1:3 herringbone patterns are $\sigma_t = \frac{0.5 + \mu}{4} \sigma_c$, and $\sigma_t = \frac{1/3 + \mu}{3} \sigma_c$ respectively. σ_t , σ_c , and μ indicate the crosswise tension resistance, the vertical compressive stress, and the friction coefficient respectively. My aim was to check these predictions with computer-simulated experiments.

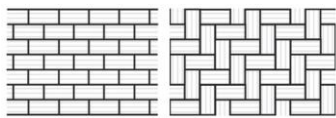


Figure 1.2. The basic bond types for masonry shells: running bond (left) and herringbone (right).

1.3 Validation of the theoretical predictions

I studied cylindrical walls (Figure 1.3) subjected to uniformly distributed vertical compressive stresses and gradually increasing distributed outwards pressure on intrados to validate the theoretical predictions. The outwards pressure was applied in a quasi-static manner (the structure was carefully equilibrated after each load increase) until a further increase in pressure could no longer be reached. My results (Figure 1.4) showed that the theoretical predictions were always slightly conservative. The deviations between the prediction and numerical experiments did not exceed 10% and were usually much smaller.

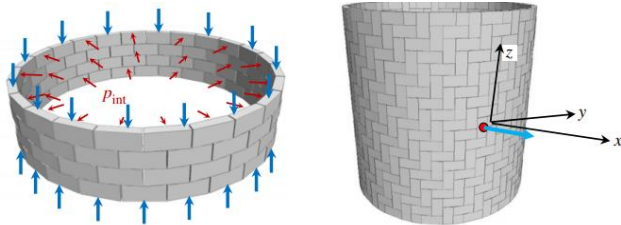


Figure 1.3. Cylindrical walls: running bond (left) and herringbone patterns (right).

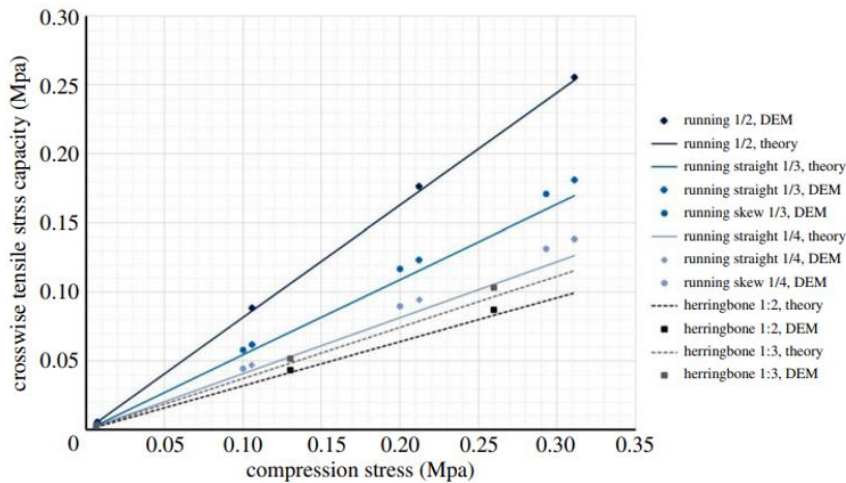


Figure 1.4. Dependence of hoop tensile strength on vertical compression.

Thesis 2: DEM analysis of masonry hemispherical domes externally reinforced by metal bars

2.1 Introduction

The typical cracking of a hemispherical dome is “orange-slice” cracking (Figure 2.1a). The magnitude of the crack opening or width at the base level is the largest if the bottom of the dome is free to translate outwards. However, the location of maximum crack opening also depends on the boundary conditions. For example, if a dome is fixed at the base level (e.g., a dome stands on the ground), then the largest crack opening (Figure 3.1.b) occurs above the base level. In reality, reinforcement is often applied to prevent the orange-slice-like cracking. However, the behaviour of a reinforced hemispherical dome is not well understood (Varma et al., 2018), and in particular, the optimal location of reinforcement is still an open issue. Even though few researches such as

Chiozzi (2016) and Varma & Ghosh (2015) studied the optimal location of the reinforcement for a hemispherical dome by using FEM, the discontinuity of masonry domes and the boundary effects were neglected.

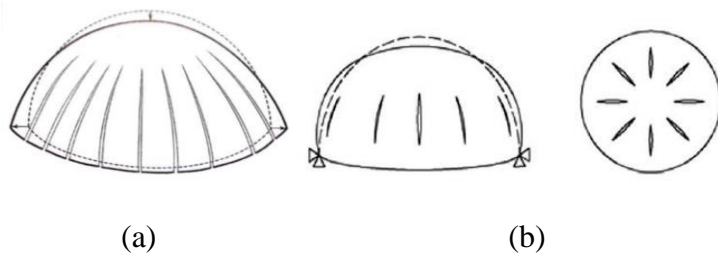


Figure 2.1. Cracking of hemispherical domes: (a) “Orange-slice” cracking without supporting, and (b) “Orange-slice” cracking when dome is fixed at bottom (Atamturktur et al., 2012).

2.2 Numerical simulations

I investigated two hemispherical domes (with $t/R = 0.049$ and 0.098 , where t and R denote the thickness and the radius of the middle surface of the dome). The dome consisted of 50 individual lunes around its perimeter, and 18 horizontal rings of stone blocks. I applied stacked bond pattern to exclude the effect of crosswise tensile resistance. Reinforcement was placed at the mid-position of the selected ring and installed on the extrados of the dome at various positions. The optimal location of the reinforcement is determined by the angle α , measured from the bottom (Figure 2.2). The optimal location is defined by the ratio of F_h/F_v , where F_h and F_v indicate the horizontal and vertical reactions at the base level (Figure 2.3), and the location of the maximum crack appeared on the dome. A smaller F_h/F_v ratio indicates a reduced risk of the underlying supporting structures being endangered by tilting. Boundary conditions of the studied domes were represented by the heights (Figure 2.4) and thicknesses of the drums. The significance of contact cohesion was simulated by applying the parameters of cohesion c and tensile strength σ_t in the contacts between blocks. The relation between them was defined as $\sigma_t = c/\tan\phi$.

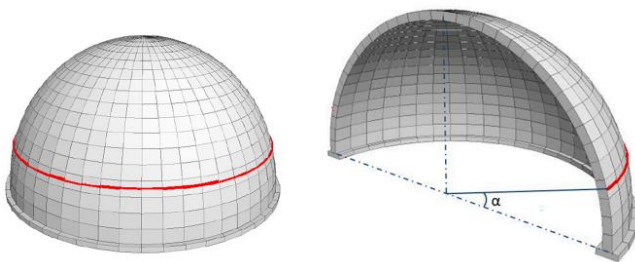


Figure 2.2. The analyzed dome in 3DEC: dome installed with reinforcement (left) and illustration of the reinforcement location (right).

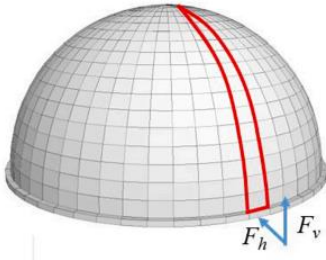


Figure 2.3. The horizontal F_h and vertical F_v reaction forces at the base.

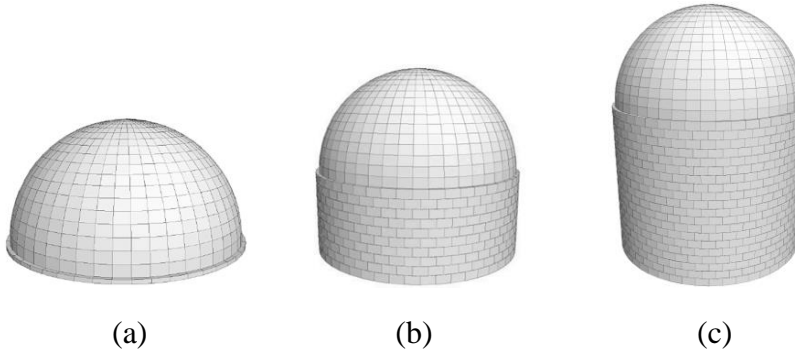


Figure 2.4. The analyzed dome with different boundary conditions: (a) dome with fixed support, (b) dome on a 5.0m high drum, and (c) dome on a 10.0m high drum.

The results showed that by increasing the normal stiffness of the reinforcement, increasing the height or decreasing the thickness of drums, and adding contact cohesion, the optimal location of the reinforcement moved closer to the base level.

Thesis 3: DEM analysis of masonry open vaults with square bays

3.1 Introduction

Historic masonry vaults and domes are often considered as the revolutions of smooth curves. The curved geometry of these shells introduces complex mechanical behaviours. A key characteristic of curved shells is their Gaussian curvature, which has significant implications for their structural behavior, including load-carrying capacity and failure mechanisms. Vaziri & Mahadevan (2008) analyzed the deformation in a toroidal continuum (Figure 3.1) shell by using Abaqus. It was found that for surfaces with zero and positive Gaussian curvatures, the deformation of the shell submitted to a concentrated force is localized around a small region where the concentrated load is applied. However, when a load is applied to a surface with a negative Gaussian curvature, the deformation extends through the entire system. Despite these insights, the mechanical effects of the sign of Gaussian curvature in masonry shells (discontinuum shells) remain poorly understood. Further research is needed to fully comprehend these effects.

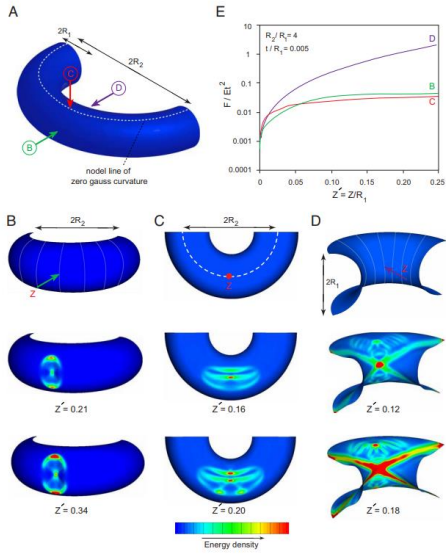


Figure 3.1. Indentation of a toroidal shell: (A) schematic of a segment of a toroidal shell; (B) deformation caused by normal indentation of the point on the outer surface, which has positive Gaussian curvature; (C) deformation caused by normal indentation of the point on the nodal line, which has zero Gaussian curvature; (D) deformation caused by normal indentation of the point on the inner surface, which has negative Gaussian curvature; and (E) force-indentation response of the three shells under indentation (Vaziri and Mahadevan, 2008).

3.2 Numerical simulations

I analyzed three types of masonry shells (Figure 3.2)—sail vaults, fan vaults, and cross vaults—representing positive, negative, and zero Gaussian curvatures respectively, to investigate the effect of Gaussian curvature on load-bearing capacity, failure mechanisms, and the orientation of reactions at supports. The analysis considered vertical concentrated loads at three characteristic points (Figure 3.3a) on the vaults and outward support displacements (Figure 3.3b) to understand these effects. I also adopted a combined approach to model those vaults where wall separation had already occurred. All the loads were applied in quasi-static manner. Vaults with 10cm and 16cm thicknesses were studied for comparison.

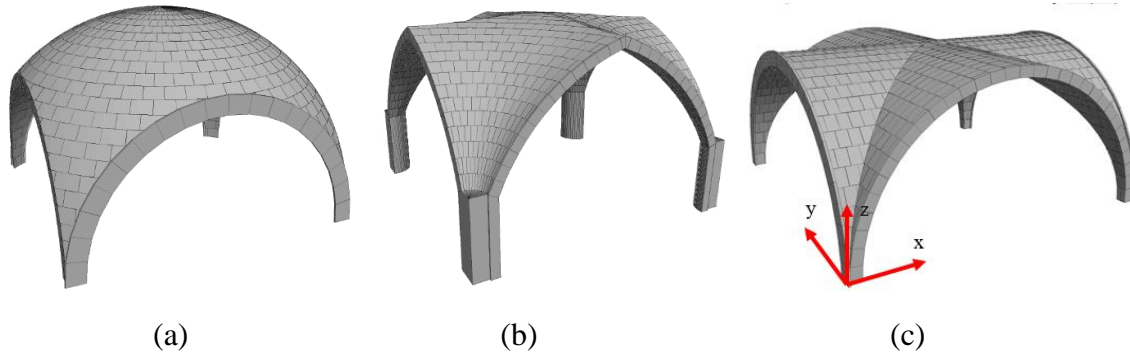


Figure 3.2. Geometries of the analyzed vaults in 3DEC: (a) sail vault, (b) fan vault, and (c) cross vault.

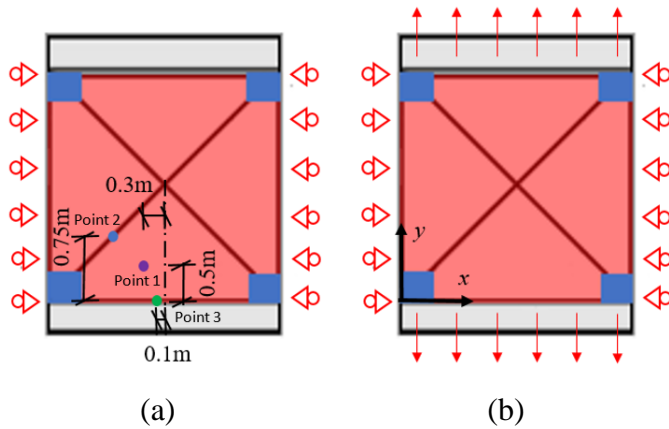


Figure 3.3. The boundary conditions and loading cases: (a) vertical loads, and (b) outwards support displacement.

The results showed that under concentrated loads, only local failure occurred in the masonry shell with positive Gaussian curvature (sail vault). In contrast, the failure mechanisms of the shells with negative and zero Gaussian curvatures depended on the loading positions. All vaults exhibited global cracks under outwards support displacement. The cracking patterns of the vaults under concentrated loads were not influenced when initial wall separation had already occurred, but the load-bearing capacity dramatically decreased due to the loss of lateral support from the longitudinal wall.

Thesis 4: DEM analysis of the load-bearing capacity of barrel vaults under vertical loads

4.1 Introduction

Barrel vaults are the simplest form of historic vaults. Over the centuries, master builders have used four distinct patterns (Figure 4.1) to construct barrel vaults. Among these, longitudinal and transverse vaults (Figures 4.1a and 4.1b) are the most widely used patterns.

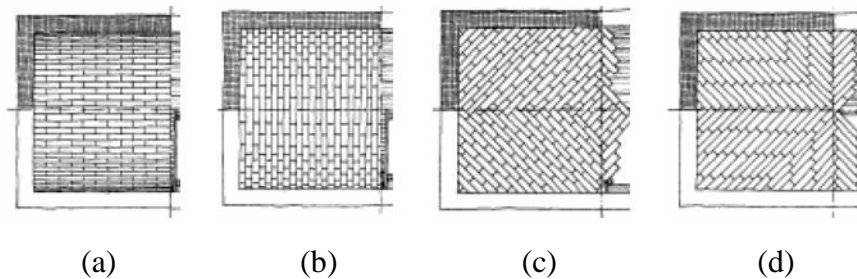


Figure 4.1. Existing bond patterns for a barrel vault: (a) longitudinal vault, (b) transversal vault, (c) bone vault, and (d) inverted bone vault (Levi, 1932).

This study, carried out in cooperation with two Italian researchers (A. Ferrante and F. Clementi), was inspired by Romano & Grande (2008), who applied the finite element method (FEM) to analyze the mechanical response of barrel vaults with longitudinal and transverse patterns. Their

findings indicated that under concentrated loads, the load-bearing capacity of longitudinal barrel vaults is higher than that of transverse barrel vaults. However, their study did not consider the failure modes, specifically the sliding and separation of the blocks, which are critical to understanding the structural behaviour of these vaults under load. Additionally, they did not address the importance of the size effect (an arch that consists of a lower number of blocks along the arc has a greater load-bearing capacity than an arch with the same geometry but consists of a larger number of blocks shown in Figure 4.2) of the blocks, which is also a significant factor in the structural performance of barrel vaults.

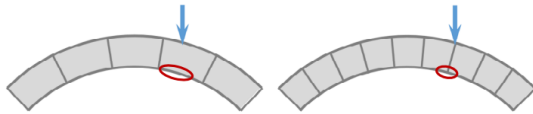


Figure 4.2. Size effect of the voussoir length along the arc: arch with larger size of blocks (left) and arch with smaller size of blocks (right).

4.2 Numerical simulations

My task in the team was to do virtual experiments on the effect of bond pattern on the load bearing capacity of barrels. The geometrical characteristics of the blocks and their material properties were provided by the Italian partners, and my task was to prepare the vault models and then run the simulations. Transversal and longitudinal barrel vaults with three different angles of embrace (180° , 120° and 60°) were investigated. The middle span of each barrel vault was 2.4m, and the thickness was 0.15m. The length of the short barrel vault was 1.24m (Table 4.1) in the longitudinal y direction. For the long barrel vault, the length was 4.65m.

Table 4.1. Geometries of barrel vaults with a 1.24 m span.

Angle of embrace	Middle radius	Intrados radius	Extrados radius	Transverse barrel vaults	Longitudinal barrel vaults
180°	1.2 m	1.125 m	1.275 m		
120°	1.386 m	1.311 m	1.461 m		
60°	2.4 m	2.325 m	2.475 m		

Three different loading approaches (Figure 4.3) were considered: 1) concentrated loading at $1/3$ of the length; 2) distributed loading along the whole length; and 3) a square distributed loading around the region at $1/3$ of the length of the barrel vaults.

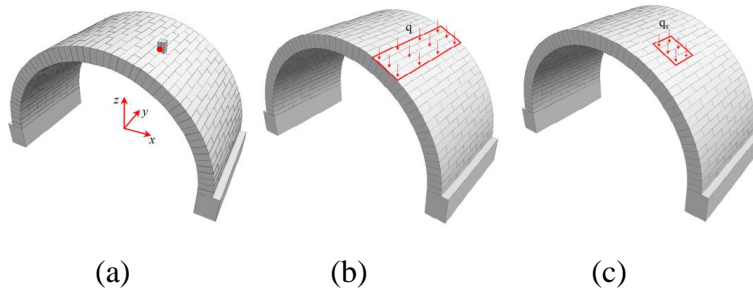


Figure 4.3. Loading methods: (a) concentrated loading, (b) full-length distributed loading, and (c) square distributed loading applied for longitudinal barrel vaults with 180° embrace angle.

The results showed that under concentrated and square distributed loads, only local failure occurred in the transversal barrel vaults. In contrast, the entire longitudinal barrel vaults failed due to hinge cracks along their entire length. Under loads distributed along the entire length of the vaults, the transversal barrel vaults exhibited a larger load-bearing capacity compared to the longitudinal barrel vaults. Additionally, the size effect (decreasing the number of blocks along the arc) in transversal barrel vaults increased their load-bearing capacity.

Thesis 5: DEM analysis of fan vaults

5.1 Introduction

In many fan vaults, there is a small space outside the extrados and above the tas-de-charge, named “vaulting pocket”. This space is often filled with rubble stones (Figure 5.1). The backfill height is approximately $1/2$ – $2/3$ of the total height of the vault (Leedy, 1980). The mechanical role of the backfill in fan vaults is an open issue for analysis (Bagi, 2021).

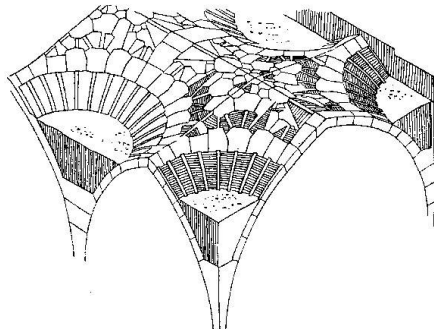


Figure 5.1. A fan vault with rubble stone backfill

5.2 Numerical simulations

I studied fan vaults with spans of 3.0 meters and 5.2 meters, each with a thickness of 10 cm which is a typical thickness for historic fan vaults. Given that only self-weight and outward support displacement were considered, and taking into account the symmetry, only one-fourth of a complete fan vault was studied. For the vault with a 3.0-meter span, an extremely small thickness of 2.5cm was also investigated for comparison. The backfill was modeled using Voronoi elements

(Figure 5.2), and different heights of backfill were generated to study the influence of the presence and height of the backfill on the orientation of reactions (F_y/F_z , shown in Figure 5.3) at supports. A smaller F_y/F_z ratio indicates a reduced risk of the underlying supporting structures being endangered by tilting.

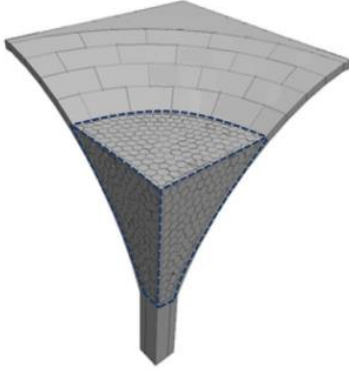


Figure 5.2. Fan vault with backfill (Voronoi elements).

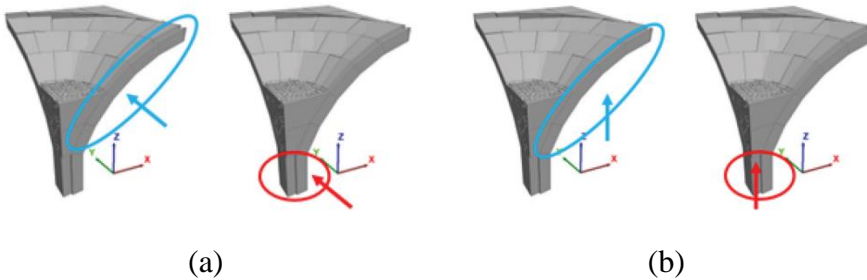


Figure 5.3. Reaction forces at the tas-de-charge and longitudinal walls: (a) F_y and (b) F_z .

The results showed that even fan vaults with extremely small thicknesses can achieve equilibrium under self-weight without any cracks. No minimum thickness was identified for the investigated fan vaults. Increasing the height of the backfill brought the orientation of reactions at the tas-de-charge much closer to vertical.

Principal results

Principal result 1

With computer-simulated experiments, I validated the theoretical predictions of crosswise tension resistance for different running bond and herringbone patterns with a realistic friction coefficient $\mu=0.781$. With deviations below 10% between theoretical predictions and numerical experiments and the theoretical predictions being always on the safe side, I showed that:

- The crosswise tension resistance of straight-shifted and skew-shifted running bond patterns for

$\alpha = 1/2, /3$ and $1/4$, is $\sigma_t = \mu \frac{\alpha b}{h} \sigma_c$.

The parameter α expresses the ratio of shifting.

- Shells with herringbone pattern also exhibit crosswise tension resistance, though their failure mode is different from that of running bond patterns. I identified two failure modes, depending on the magnitude of friction coefficient on the surfaces. For 1:2 herringbone pattern, the combined rotating and sliding failure mode appears when the realistic $\mu=0.781$ friction coefficient is applied; for 1:3 herringbone pattern, the combined failure happens in this case. When $\mu= 1.235$ and 1.732 , pure tipping over failure mode occurs in 1:3 herringbone pattern.

- The crosswise tension resistances of 1:2 herringbone and 1:3 herringbone patterns are $\sigma_t = \frac{0.5+\mu}{4}\sigma_c$, and $\sigma_t = \frac{1/3+\mu}{3}\sigma_c$ respectively, for the mixed failure mode.

In the above formulas σ_t denotes the crosswise tension resistance, σ_c is the vertical compressive stress, μ is the friction coefficient.

Related publications: [HT1], [HT6], [HT7].

Principal result 2

With computer-simulated experiments of the reinforcements of stone hemispherical domes, I showed that:

- The normal stiffness of the cross-sections of the reinforcement affects the optimal location. When the normal stiffness of the cross-sections increases, the optimal location of the reinforcement tends towards the base.
- The drum height and drum thickness affect the optimal location of the reinforcement. Reducing the thickness of the dome is equivalent to increasing the height of the drum. When the drum height increases, or the drum thickness decreases, the optimal location of the reinforcement tends towards the base.
- The existence of the resistance of the contacts to tension affects the optimal location of the reinforcement. When the contacts are cohesive, the optimal location of the reinforcements is closer the base. Moreover, the existence of tensile resistance in the contacts decreases the relative efficiency of the reinforcement.

Related publications: [HT2].

Principal result 3

With computer-simulated experiments of three basic types of open vaults, I showed that:

- Under a concentrated downwards force load, the masonry sail vault, characterized by a positive Gaussian curvature ($K > 0$), shows localized failure where only the loaded block drops out from

the initial position. Changing the loading position has no influence in the failure mode of the analyzed sail vault: it remains local.

- The masonry fan vault, characterized by a negative Gaussian curvature ($K < 0$), shows global damage. The position of the vertical loads of the fan vault affects whether the whole structure will collapse, or only the whole structure cracks but does not collapse.
- The masonry cross vault, characterized by zero Gaussian curvature ($K = 0$), shows a local failure where the loaded block drops off and some neighbouring blocks slightly move out from their original positions when the load is applied on the diagonal and near the longitudinal wall. The remaining structure is slightly cracked but can find the equilibrium with no further collapse. When the load is applied on the shell surface between the diagonal and longitudinal wall, a more extended collapse (due to the formation of a hinge line) occurs, which affects only the loaded barrel.

Related publications: [HT3].

Principal result 4

With computer-simulated experiments of transverse and longitudinal barrel vaults, I showed that:

- For short transverse barrel vaults, the failure always occurs only at the arches where the vertical loads are applied. For short longitudinal barrel vaults, the failure is because of the hinge cracking along the whole length for all analyzed loading distributions.
- For long transverse barrel vaults, the failure mechanism is the same as the short vaults. However, for long longitudinal barrel vaults, the failure mode is different. The embrace angle affects the failure mode: when the embrace angle is 180° , there is a global hinge along the whole length; when the embrace angles are 120° and 60° , the loaded blocks fall out from its own positions. The hinge will also occur, however, it is not along the whole length.
- The size effects for the transverse barrel vaults with 60° embrace angle is significant: the load-bearing capacity for the vaults with 8-bricks discretization along the arc is more than twice as the vaults with 34-bricks discretization.

Related publications: [HT4].

Principal result 5

With computer-simulated experiments of fan vaults, I showed that:

- For both small and large span fan vaults, no optimal height of the backfill exists. The higher the backfill is, the more stable the fan vault is (the orientation of reactions is closer to the vertical).
- For the small span fan vaults, the vault with larger thickness is more stable than the vault with smaller thickness. However, even the vault with the unrealistically small thickness can still find the equilibrium state under self-weight, and does not collapse even at relatively large outwards

support displacement (1.67% of the total span). There is no practical lower limit for the shell thickness for self-weight for this type of fan vault.

- The longitudinal wall expresses lateral reaction to the conoid of fan vault under self-weight only in case of fixed supports, but this contribution drops to a negligible value as soon as outwards support displacements reach the slight value of 0.02% of the span.

Related publication: [HT5].

Publications of the candidate related to the principal results

Journals:

[HT1] Chen S., Bagi K. (2020), Crosswise tension resistance of masonry patterns due to contact friction, *Proceeding of the Royal Society A* 476: 2240. doi: 10.1098/rspa.2020.0439

[HT2] Chen S., Bagi K. (2023), DEM analysis of masonry hemispherical domes externally reinforced with metal bars, *Engineering Structures* 291: 116496.

<https://doi.org/10.1016/j.engstruct.2023.116496>

[HT3] Chen S., and Bagi K. (2024), DEM analysis of masonry open vaults with square bays, submitted to *International Journal of Architectural Heritage* (under review).

[HT4] Chen S., Ferrante A., Clementi F., and Bagi K. (2021), DEM analysis of the effect of bond pattern on the load bearing capacity of barrel vaults under vertical loads, *International Journal of Masonry Research and Innovation* 6(3): 346-373.

doi: 10.1504/IJMRI.2021.116234

[HT5] Chen S., Bagi K. (2022), DEM analysis of the mechanical role of backfill of jointed masonry fan vaults: Results of virtual experiments, *International Journal of Architectural Heritage* 18 (1): 64-83. <https://doi.org/10.1080/15583058.2022.2104142>

Conferences:

[HT6] Chen S., Bagi K. (2019), Crosswise tension resistance of walls with different bond patterns, *CMN 2019 STI*, Lourenço, Flores, Clain, Greiner, Arias & Tur (eds.), ISBN: 978-989-54496-0-6, Guimarães, Portugal.

[HT7] Chen S., Bagi K. (2020), 3DEC analysis of crosswise tension resistance in masonry structures, *Proceedings of Fifth International Itasca Symposium 2020*, Billiaux, Hazzard, Nelson & Schöpfer (eds.), ISBN 978-0-9767577-5-7, Vienna, Austria.

References

- Bagi K. (2021), Statics of fan vaulting: current state of knowledge and open issues, *Proceedings of the Royal Society A*. 477(2246):20200893, 24.
- Atamturktur S., Li T., Ramage M.H., and Farajpour I. (2012), Load carrying capacity assessment of a scaled masonry dome: Simulations validated with non-destructive and destructive measurements, *Construction and Building Materials* 34:418-429.
- Beatini V., Royer-Carfagni G., and Tasora A. (2018), The role of frictional contact of constituent blocks on the stability of masonry domes, *Proceedings of the Royal Society A*. 474:20170740.
- Chiozzi A., Milani G., Grillanda N., and Tralli A. (2016), An adaptive procedure for the limit analysis of FRP reinforced masonry vaults and applications, *Am J Eng Appl Sciences* 9(3):735-45.
- Heyman J. (1967), On shell solutions of masonry domes, *International Journal of Solids and Structures* 2, 227-240.
- Leedy W. C., Jr. (1980), *Fan vaults: A study of form, technology and meaning*, Farnham: Ashgate Publishing Group.
- Levi C. (1932), *Trattato teorico pratico di costruzioni civili, rurali, stradali e idrauliche*, Hoepli, Milano, Italy.
- Romano A., and Grande E. (2008), Masonry barrel vaults: influence of the pattern, *Procs. of the 14th World Conference on Earthquake Engineering*, Beijing, China, 12-17 October.
- Simon J., and Bagi K. (2016), DEM analysis of the minimum thickness of oval masonry domes, *International Journal of Architectural Heritage* 10:457-475.
- Varma MN., and Ghosh S. (2015), In: *Effect of tension rings on the stability of axisymmetric masonry domes*, Stirlingshire: Civil-Comp Press, pp 57-71.
- Varma M. N., Ghosh S., and Milani G. (2018), Finite element thrust line analysis of cracked axisymmetric masonry domes reinforced with tension rings, *Int J Masonry Res Innovation* 3(1):72-87.
- Vaziri A., and Mahadevan L. (2008), Localized and extended deformations of elastic shells, *PNAS* 105(23).